From 8- to 18-Cluster Electrons Superatoms: Evaluation via DFT Calculations of the Ligand-Protected W@Au(12)(dppm)(6) Cluster Displaying Distinctive Electronic and Optical Properties

Jianyu Wei, Desmond Macleod-Carey, J.-F. Halet, Samia Kahlal, Jean-Yves Saillard, Alvaro Muñoz-Castro

On Heteronuclear Isoelectronic Alternatives to $Au_{13}(dppe)_5Cl_2$: Electronic and Optical Properties of the *18-electron* $Os@Au_{12}(dppe)_5Cl_2$ Cluster from Relativistic DFT Computations

Jianyu Wei,[a] Peter L. Rodríguez-Kessler,[b] Jean-François Halet,[a,c] Samia Kahlal,[a] Jean-Yves Saillard,[a] and Alvaro Muñoz-Castro[b]**

[a] Univ Rennes, CNRS, Institut des Sciences Chimiques de Rennes (ISCR) – UMR 6226, F-35000 Rennes, France

[b] Grupo de Química Inorgánica y Materiales Moleculares, Facultad de Ingenieria, Universidad Autonoma de Chile, El Llano Subercaseaux 2801, Santiago, Chile

[c] CNRS-Saint Gobain-NIMS, UMI 3629, Laboratory for Innovative Key Materials and Structures (LINK), National Institute for Materials Science (NIMS), Tsukuba, 305-0044, Japan

Abstract

The development of well-defined atomically-precise heteronuclear nanoclusters passivated by protecting-ligands is presently a booming area, owing to the fact that doping well-known homonuclear nanostructures allow fine tuning of their properties. Herein, we explore by means of DFT calculations the possibility of doping the central gold atom in the classical $[Au_{13}(dppe)_5Cl_2]^{3+}$cluster (**1**) by Os. Although both $[Au_{13}(dppe)_5Cl_2]^{3+}$ and $[Os@Au_{12}(dppe)_5Cl_2]$ have the same total number of electrons, we show that they are not isoelectronic within the formalism of the *superatom* model, being respectively a 8- and a 18-electron species. It results that they exhibit similar structures, but present significantly different optical behaviors (UV/Vis and circular dichroism). Similar results are obtained for the Ru and Fe relatives. Emission properties indicate some red-shift of the $T_1 \rightarrow S_1$ decay with respect to $[Au_{13}(dppe)_5Cl_2]^{3+}$, involving an equatorial distortion of the $Au_{12}Cl_2$ core in the T_1 state, rather than the axial distortion afforded by **1**. The sizable HOMO-LUMO gaps found for the three doped species suggest that further experimental exploration of different stable doped species derived from the ligand-protected $Au_{12}Cl_2$ core should be encouraged.

* jean-yves.saillard@univ-rennes1.fr and alvaro.munoz@uautonoma.cl

Introduction

The fastly developing chemistry of gold nanoclusters (AuNCs) is currently of huge topical interest owing to their many potential interdisciplinary applications,[1–20] Numerous theoretical and experimental research efforts have contributed to the rationalization of their structure and the viability of novel noble-metal nanostructures.[21–38] The most recent developments of this field encompass the design of doped AuNCs,[39–48] an efficient strategy to tune the properties of the parent homonuclear clusters.[24,25,44,49–57]

AuNCs consist of atomically precise metallic cores further passivated by a protecting shell of ligand, to which in some cases are added additional Au(I) centers.[58–62] The Au_{13} icosahedron is one of their most recognizable motifs as earlier characterized in the very first phosphine derivatives $[Au_{13}(PMe_2Ph)_{10}Cl_2]^{3+}$ by Mingos and coworkers[63] and later in $[Au_{13}(dppe)_5Cl_2]^{3+}$ (**1**),[64,65] precluding the most recent extensive research on $[Au_{25}(SR)_{18}]^-$,[66–70] which have been extended to other related clusters.[53,71–75] In the last decade compound **1** has been further explored revealing its interesting optical and chiroptical properties as investigated separately by Konishi[64] and Li,[64,65] showing an enhanced behavior compared to other phosphine-protected clusters.[76–78] In addition, the high quantum yield of the lowest triplet state (T_1) leads to promising singlet-oxygen ($^1O_2$) photogeneration capabilities in comparison to organic dyes such as by anthracene, as well as related $Au_{25}(SR)_{18}$ and $Au_{38}(SR)_{24}$ clusters .[79,80]

Within the *superatom* model,[53,58,74] **1** is described as a 8-cluster-electron (8-*ce*) species. Indeed, only the electrons significantly involved in metal-metal bonding, that is the 6s(Au) valence electrons of the $[Au_{13}]^{5+}$ core, are included in the *superatom ce* count. The 5d(Au) electrons are not considered for they have been recognized a long time ago to play a negligible role.[81] The highest occupied orbitals of **1** correspond to the 1P shell[58,82,83] and the lowest unoccupied levels to the 1D manifold. The 1P→1D electronic transitions account for the character of the low-energy UV/Vis spectrum and the related luminescent properties. In this context, the exploration of 18-*ce* related counterparts allows further understanding of the role of electron counts in the optical properties, based on heteroatom doping of the cluster-core,[24,84–88] as earlier theoretically proposed and experimentally demonstrated by the bare $W@Au_{12}$ cluster by Pyykkö and Li, respectively.[89,90]

A proper candidate is given by doping the parent cluster **1** by Os resulting in a neutral 18-*ce* $[OsAu_{12}(dppe)_5Cl_2]$ (**2**) species (assuming that Os lies at the cluster center,

see below). It is important at this stage to note that although $[Au_{13}(dppe)_5Cl_2]^{3+}$ (**1**) and 18-*ce* (**2**) are isoelectronic in terms of their total and valence number of electrons, within the *superatom* model, we suggest considering them as respectively *8-ce* and *18-ce* species. This difference originates in the fact that the fully occupied 5d(Au) orbitals are low-lying and contracted, whereas the 5d(Os) ones are higher in energy and more diffuse. Therefore, contrarily to the former, the latter can participate to cluster bonding. This is why we include the 5d electrons of Os into the *ce* count of (**1**), whereas in (**2**) we do not include that of the encapsulated Au. Likewise, the naked $W@Au_{12}$ cluster is also commonly considered as a 18-*ce* species .[89,90] We thus consider **2** as having the $1S^2$ $1P^6$ $1D^{10}$ configuration, with 1D HOMOs (or near HOMOs) of large 5d(Os) nature, giving rise to optical properties different from that of **1**, whose configuration is $1S^2$ $1P^6$. These different situations are sketched in Scheme 1, where the *superatomic* electronic structures of $M@Au_{12}$ (M = Au, Os) cores are showns on the basis of the interaction of M with its M_{12} icosahedral cage.

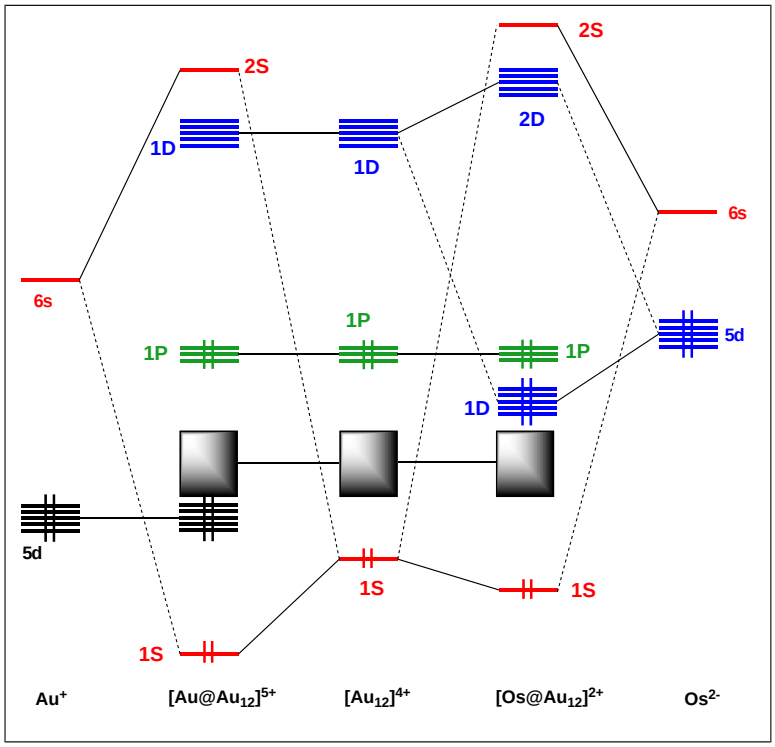

Scheme 1. Interaction of a formally d^{10} encapsulated metal atom M with an icosahedral $[Au_{12}]^{4+}$ icosahedral cage. Left: M = gold; right: M = osmium. Note that the $[Os@Au_{12}]^{2+}$ case is similar to that of $[W@Au_{12}]$.[81,82]

Obviously, the two situations crudely illustrated in Scheme 1 should be considered as two limit cases and there should be a gradual transition between them, *i.e.*

when going from W to Au. Thus, the description of a $[M@Au_{12}]^{n+}$ (M = W, Au; n = 0, +5) cluster core as a 18-*ce* rather than a 8-*ce* species (or conversely) is somewhat formal. From the relativistic density functional (DFT) calculations described below, we suggest placing the formal 18-*ce*/8-*ce* borderline on the right side of Os. In this investigation, the stability and bonding patterns of the hypothetical cluster **2** are explored and its electronic, optical, chiroptical and potential luminescent properties are analysed, with systematic comparison with its homonuclear parent **1**. The isoelectronic clusters $[MAu_{12}(dppe)_5Cl_2]$ (M = Fe, Ru) are also discussed. As we were working on these hypothetical species, the isolation and full characterization of $[IrAu_{12}(dppe)_5Cl_2]^+$ and $[PtAu_{12}(dppe)_5Cl_2]^{2+}$ were published by Tsukuda and coworkers,[91] thus supporting the fact that the hypothetical title Os species is feasible.

Computational Details

Calculations were carried within the Density Functional Theory[92] (DFT) formalism using the ADF2019 code.[93] Scalar relativistic corrections via the ZORA Hamiltonian were considered[94] together with the generalized gradient approximation (GGA) Perdew-Burke-Ernzerhof (PBE) exchange-correlation (xc) functional,[95,96] owing to its reliable performance at reasonable computational cost on AuNCs.[83,97–100,89] Dispersion forces were considered via the empirical pairwise corrections of Grimme (DFT-D3).[101] Basis sets of triple-ξ Slater quality, plus two polarization functions (STO-TZ2P) were employed for valence electrons. The frozen core approximation was applied to the $[1s^2\text{-}4f^{14}]$ shells for Au and Os, $[1s^2\text{-}4p^6]$ Ru, $[1s^2\text{-}3p^6]$ Fe, $[1s^2]$ for C, and $[1s^2\text{-}2s^2]$ for P and Cl, leaving the remaining electrons to be treated variationally. Ground and excited states geometry optimizations were performed without any symmetry constraint, via the analytical energy gradient method implemented by Versluis and Ziegler,[102] with energy convergence criteria set at 10^{-4} Hartree, gradient convergence at 10^{-3} Hartree/Å and radial convergence of 10^{-2} Å. Electronic excitation energies were calculated via time-dependent-DFT (TD-DFT) considering the van Leeuwen–Baerends (LB94) xc-functional as in previous similar studies.[46,100,103] The current approach was tested on the description of dual photoluminescence properties of a ligand-supported hexanuclear Au(I) framework, with good agreement to experimental emission and absorption energies.[104]

Results and Discussion

The question of the location of heteroatoms in doped group 11 metal clusters has been first addressed in 1989.[105] In the case of **1,** doping it by formally replacing one Au atom by Os (keeping constant the total electron number) results in three possible configurations for **2**. One with Os on the central site (isomer **I**), another one with Os bonded to a dppe ligand (isomer **II**) and the third one when bonded to chlorine (isomer **III**). The resulting optimized structures (Figure 1) indicate a large preference for isomer **I**, being largely favored by +99.1 and +101.0 kcal.mol^{-1} with respect to isomers **II** and **III**, respectively. This is consistent with the fact that only isomer **I** can be described as a superatom with *18-ce* count (see above). This observation agrees with the recently published structures of the closely related compound $[IrAu_{12}(dppe)_5Cl_2]^{+}$.[91] Thus, hereafter, we refer our results to isomer **I** for **2**. The relaxed structures of **1** and **2** exhibit similar $M_{(center)}$-$Au_{(ligand)}$ distances of 2.622 and 2.612 Å, respectively, which compares well to experimental data available (2.552 Å) for **1** (Table 1).[64] The calculated $M_{(center)}$–$Au_{(Cl)}$ distance in **2** (2.596 Å) is slightly enlarged in comparison to those in **1** (from 2.548 to 2.596 Å). Similar Au–Cl separations (from 2.201 to 2.288 Å) are computed for **1** and **2**, denoting that the $Au_{12}Cl_2$ cage remains similar upon osmium doping.

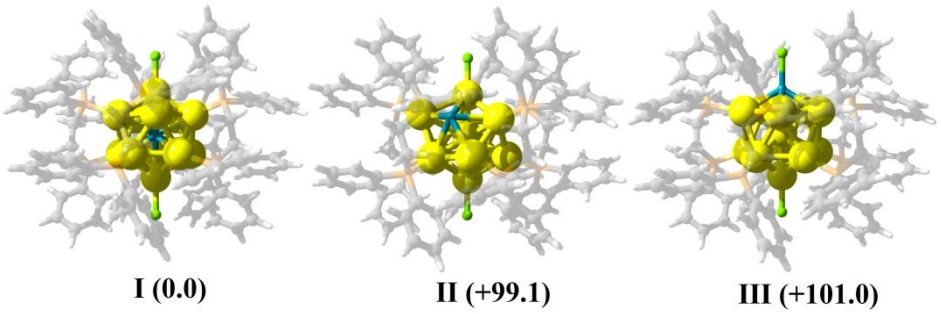

Figure 1. Relaxed structures of the three isomers **I-III** of $[OsAu_{12}Cl_2(dppe)_5]$ (**2**). Relative energies are given in brackets (kcal.mol^{-1}). Os atom is in blue.

Table 1. Structural parameters for $[M@Au_{12}(dppe)Cl_2]^{n+}$ species (M = Au, n = 3; M = Os, Ru, Fe, n = 0).

	Exp Au[a]	Au (**1**)	Os (**2**)	Ru	Fe
$M_{(center)}$–$Au_{(ligand)}$	2.552	2.622	2.612	2.623	2.624
$M_{(center)}$–$Au_{(Cl)}$	2.486	2.548	2.596	2.608	2.483
Au–Cl	2.169	2.201	2.288	2.307	2.331

[a]Experimental data from ref.[64]

The electronic structures of **1** and **2** are illustrated in Figure 2. The occupied 1D shell of **2** is intercalated between the $1P_{x,y}$ HOMOs and $1P_z$ superatomic orbitals (shell splitting allowed by symmetry). In average, the 1D shell of **2** is composed of 52% 5d(Os) character mixed in a bonding way with 21% 6s/6p(Au), and 27% from protecting ligands. Such an occupied $5d(M_{(center)})$ shell does also exist in **1**. However, these low-lying combinations are fully non-bonding, with no significant $6s/6p(Au_{(ico)})$ admixture and thus cannot be considered as the superatomic 1D shell. Rather, the true 1D orbitals of **1** are its five lowest vacant ones, which are of dominant 6s/6p(Au) composition, with $Au_{(center)}$–$Au_{(ico)}$ bonding character (Figure **2**). On the other hand, the lowest vacant levels of **2** are not of superatomic character, but π*-ligand centered orbitals.

The singlet state of **2** is largely favored in comparison to the triplet and quintet states (by 53.2 $kcal.mol^{-1}$ and 91.9 $kcal.mol^{-1}$, respectively). Consistently, its HOMO–LUMO is large (1.53 eV) and similar to that of **1** (1.96 eV). The $[Ru@Au_{12}(dppe)_5Cl_2]$ and $[Fe@Au_{12}(dppe)_5Cl_2]$ relatives have also a substantial preference for isomer **I** (+88.7 and +128.4 $kcal.mol^{-1}$ from the next isomer, respectively, see Supporting Information). They also have significant HOMO–LUMO gaps (1.52 and 1.09 eV, respectively) and show similar frontier orbitals.

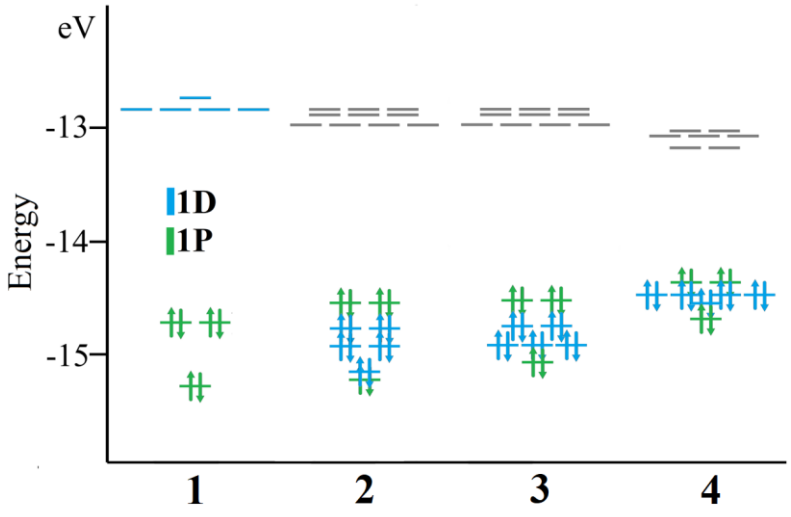

Figure 2. Electronic structure of $[Au_{13}Cl_2(dppe)_5]^{3+}$ (**1**), $[Os@Au_{12}Cl_2(dppe)_5]$ (**2**), $[Ru@Au_{12}Cl_2(dppe)_5]$ (**3**) and $[Fe@Au_{12}Cl_2(dppe)_5]$ (**4**), showing 1P and 1D superatomic shells.

In order to evaluate the variation of the interaction between the dppe ligands and the rest of the molecule, we computed the overall interaction energy (ΔE_{int}) between the [$(dppe)_5$] phosphine shell and the $[M@Au_{12}Cl_2]^{n+}$ (M = Au, n = 3; M = Os, n = 0) fragment. It amounts to -160.7 kcal.mol^{-1} for **1** and -96.5 kcal.mol^{-1} for **2** (per dppe unit). Values similar to **2** were found for the M = Ru and Fe relatives, i.e., -96.0 and -91.7 kcal.mol^{-1}, respectively. The origin of the difference in interaction energy ΔE_{int} between the homonuclear Au cluter and its heteronuclear congeners can be interpreted within the Energy Decomposition Analysis (EDA) framework given by Ziegler and Rauk,[106–108] according to:

$$\Delta E_{int} = \Delta E_{Pauli} + \Delta E_{elstat} + \Delta E_{orb} + \Delta E_{disp}$$

leading to different chemically meaningful quantities accounting for the destabilizing character of the interaction given by the repulsion between occupied orbitals (ΔE_{Pauli}), and for the stabilizing electrostatic, covalent and dispersion (charge transfer) characters, $\Delta E_{elstat,}$ ΔE_{orb} and ΔE_{disp}). The character of the interaction is mainly electrostatic, similar to other phosphine protected gold clusters.[109]

The EDA analysis shows that the stabilizing ligand-core interaction, involving one dppe ligand from $[Au_{13}Cl_2(dppe)_5]^{3+}$ to $[Os@Au_{12}(dppe)_5Cl_2]$, varies mostly by the decrease in the orbital interaction term (ΔE_{orb}) from -190.4 to -146.6 kcal.mol^{-1}, retaining a smaller variation from the electrostatic character of the interaction (-336.9 to -343.5 kcal.mol^{-1}, respectively), which accounts for the variation in the ligand-core interaction. In the Ru and Fe counterparts, a similar variation is found with ΔE_{orb} amounting to -144.0 and -144.8 kcal.mol^{-1}, respectively. The proposed 18-*ce* phosphine-protected clusters are thus structurally related to the parent $[Au_{13}Cl_2(dppe)_5]^{3+}$, with weaker ligand-core interaction energy indicating the smaller role of the protecting ligands to achieve stable species with sizable HOMO–LUMO gap, owing to the extra $1D^{10}$ electrons in the cluster core of the former. Analysis of the overall interaction energy of the $[M@Au_{12}]^{n+}$ metallic core with the whole protecting ligands shell leads to a similar trend (Supporting Information).

Table 2. Energy decomposition analysis between the [(dppe)$_5$] phosphine shell and the [M@Au$_{12}$Cl$_2$]$^{n+}$ (M = Au, *n* = 3; M = Os, Ru, Fe , *n* = 0). Values in kcal.mol^{-1}.

	1		**2**		**3**		**4**	
	Au		Os		Ru		Fe	
ΔE_{Pauli}	390.2		416.5		400.5		389.1	
ΔE_{elstat}	-336.9	61.1%	-343.1	66.9%	-329.5	66.4%	-311.9	64.9%
ΔE_{orb}	-190.4	34.6%	-146.6	28.6%	-144.0	29.0%	-144.8	30.1%
ΔE_{disp}	-23.6	4.3%	-23.3	4.5%	-23.0	4.6%	-24.1	5.0%
ΔE_{int}	-160.7		-96.5		-96.0		-91.7	

Optical properties were also addressed in order to investigate the expected differences between **1 (**8-*ce*) and **2** (18-*ce*). The experimental UV/Vis spectrum of **1** (Figure 3) features a moderate shoulder between 620 and 520 nm, followed by a more intense signal at 488 nm.[64] The calculated spectrum of **1** exhibits peaks at 590 and 473 nm accounting nicely for the experimental observation,[110] with $1P_{x,y} \rightarrow \pi^*$-ligand and $1P_z \rightarrow 1D$ transition character, respectively. In the case of **2**, several peaks appear in the calculated spectrum (Figure 3). That of lowest energy (801 nm) is associated with a $1P_{x,y} \rightarrow \pi^*$-ligand transition. It is substantially red-shifted with respect to the parent cluster **1** (590 nm). The next peak manifold is composed of five signals at 672, 642, 603, 577, and 541 nm, accounting for different $1D \rightarrow \pi^*$-ligand transitions, which are not found in the 8-*ce* parent **1**. Another peak at 499 nm is found of mixed $1D \rightarrow \pi^*$-ligand and $1P_z \rightarrow \pi^*$-ligand character, resembling the peak of **1** at 473 nm (488 nm experimentally[64]). Thus, the existence of an occupied 1D shell in **2** gives rise to a manifold peak pattern expected from the UV/Vis spectrum characterized mainly by metal $\rightarrow \pi^*$-ligand transitions, which are desired for photoinduced electron injection over surfaces from anchored gold nanoclusters.[111]

A quite similar simulated UV/Vis behavior is obtained for the Ru relative, with the first peak at 796 nm of $1P_{x,y} \rightarrow \pi^*$-ligand nature followed by a 671-542 nm manifold of $1D \rightarrow \pi^*$-ligand character with mixed $1D \rightarrow \pi^*$-ligand and $1P_z \rightarrow \pi^*$-ligand transition at 490 nm. In the case of the Fe species, the simulated spectrum exhibits a weak low-energy peak at 796 nm ($1P_{x,y} \rightarrow \pi^*$-ligand) followed by a 663-526 nm peak manifold of $1D \rightarrow \pi^*$-ligand character, with the appearance of the related $1P_z \rightarrow \pi^*$-ligand transition at 450 nm.

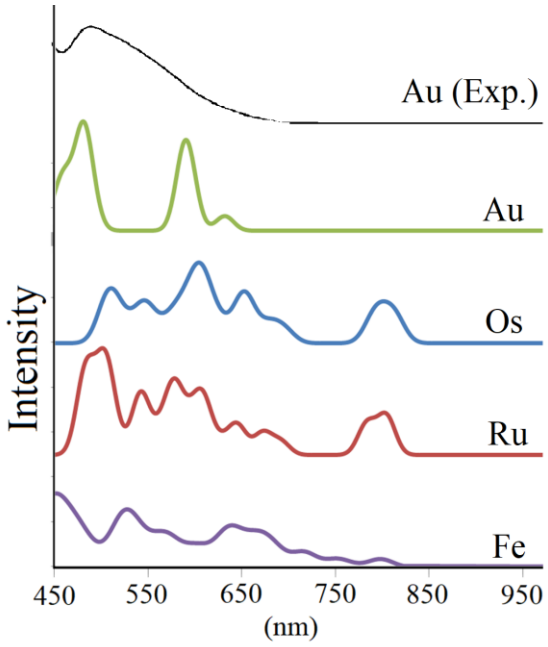

Figure 3. Calculated UV/Vis absorption spectra of $[Au_{13}Cl_2(dppe)_5]^{3+}$, and $[M@Au_{12}Cl_2(dppe)_5]$ (M = Os, Ru, Fe). The experimental spectrum of $[Au_{13}Cl_2(dppe)_5]^{3+}$ [64] is also shown for comparison.

The stereochemical constraints of the dppe ligands in **1** induce a substantial distortion of the icosahedral Au_{13} core[63–65] and their helical orientation induces some chirality, resulting in two possible enantiomers insphering circular dichroism (CD) properties. The CD spectra were computed for the right-handed enantiomers (Figure 4). That of $[Au_{13}Cl_2(dppe)_5]^{3+}$ (**1**) reproduces well its experimental CD spectrum,[64] with a positive peak at 560 nm (563 nm experimental) and a negative peak at 462 nm (472 nm experimental). That of $[Os@Au_{12}(dppe)_5Cl_2]$ (**2**) shows similar amplitudes but different shape. Its peak at 801 nm appears as a positive band, followed by another positive band peaking at 642 nm. The next peak manifold shows a negative and positive band, resulting in a pattern fingerprint different than for **1**. A pattern quite similar to that of **2** is found for its Ru and Fe counterparts, with the exception of a negative band around 800 nm for the Fe species. A comparison of the strength of the CD signal, suggest a slightly more pronunced for heterometallic species, which can be of interest for further studies.

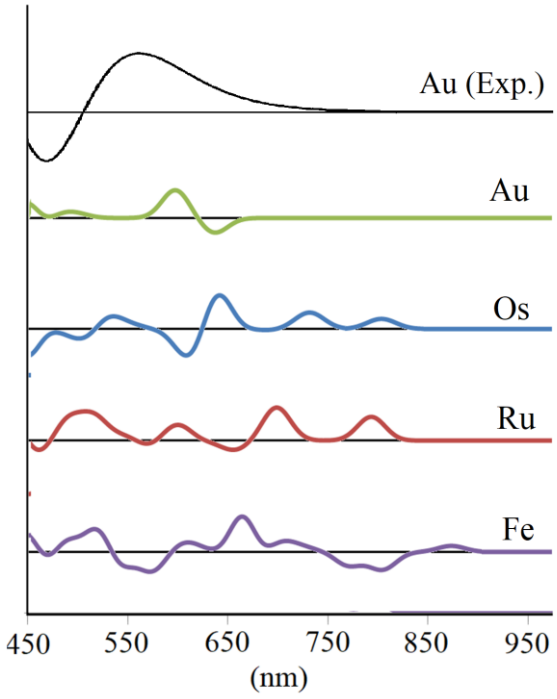

Figure 4. Calculated circular dichroism spectra for right-handed isomers of $[Au_{13}Cl_2(dppe)_5]^{3+}$, and $[M@Au_{12}Cl_2(dppe)_5]$ (M = Os, Ru, Fe). A broadening of 0.2 eV was employed. Values centered between $\pm 500 \times 10^{-40}$ $esu^2.cm^2$. The experimental spectrum of $[Au_{13}Cl_2(dppe)_5]^{3+}$ [64] is also shown for comparison.

The remarkable photoluminescent properties reported for **1**[64,65] are ascribed to a $T_1 \rightarrow S_0$ decay[64] process, providing interesting singlet-oxygen sensitization applications. For a comparison, they were also evaluated for the 18-*ce* cluster counterparts and are discussed here. The emission wavelength of **1** was found experimentally at 766 nm (1.61 eV) by Konishi and Shichibu.[65] Computations indicate a transition between the related $T_1 \rightarrow S_0$ states at the T_1 geometry at 809 nm (1.53 eV),[110] which corresponds to a 1D → 1P decay. The excited state affords an increase of the axial AuCl–AuCl distance from 5.096 (S_0) to 5.184 Å (T_1). For $[Os@Au_{12}(dppe)_5Cl_2$ (**2**) the computed emission wavelength is red-shifted to the NIR at 1045 nm (1.19 eV). This time the T_1 states retain an axial ClAu-AuCl distance (5.18 Å) similar to that in S_0), but affords a particular equatorial PAu–AuP change from 5.22 (S_0) to 5.43 Å (T_1), in contrast to the structural rearreagnments at the excited state from **1**.

The calculated emission energies of the Ru and Fe counterparts are similar, amounting to 1076 nm (1.15 eV) and 1210 nm (1.02 eV), respectively. In the case of Ru, the T_1 states exhibits also a similar axial ClAu-AuCl distance (5.180 Å) than its S_0 ground-state, (5.217 Å) but affords a particular equatorial PAu–AuP change from 5.245

(S_0) to 5.536 Å (T_1). In the case of Fe, the S_0 and T_1 states retain similar ClAu-Au-Cl distance (4.967 and 4.886 Å, respectively), but show a decrease of the PAu–AuP distance from S_0 (5.248 Å) to T_1 (5.164 Å).

Analysis of related Hg-doped species given by $[Hg@Au_{12}Cl_2(dppe)_5]^{4+}$ species, leads to the preference for isomer **III**, i.e. Hg located at the M-Cl site, suggesting the possible extension to other doped species at different sites of the MAu_{12} core, besides the central position (Supporting information).

We would like at this stage to come back to the fact that **1** and **2** are both isoelectronic and have different superatom electron counts (*18-ce* and *8-ce*, respectively). They have the same total number of cluster valence electrons (162 including the ligand lone pairs and all the 5d electrons). This electron count satisfy the rule established by Mingos in the 1980s for spherical high-nuclearity gold phosphine clusters ($12xn_s + 18$, where n_s = number of surface gold atoms).[112,113]

On the other hand, **1** and **2** are *18-ce* and *8-ce* superatoms, respectively. This difference originates from the fact that the 5d($M_{(center)}$) orbitals (and electrons) participate to the bonding in the former *but* do not participate significantly in the later (Scheme 1). As discussed in the introduction, there should be a continuum with intermediate situations when going from Os to Au, with the 10 5d($M_{(center)}$) electrons participating in an intermediate fashion to the bonding. The very recently published compounds $[IrAu_{12}(dppe)_5Cl_2]^+$ and $[PtAu_{12}(dppe)_5Cl_2]^{2+}$ are now elegantly completing the continuum series.[91] They were described by Tsukuda and coworkers as *8-ce* species, but differing from $[Au_{13}(dppe)_5Cl_2]^{3+}$ in that when doping the central position by Pt or Ir (keeping the total electron number constant)**,** the jellium core potential which controls the superatomic electron configuration becomes shallower at the central position.[91] Although different, this rationalizing approach is equivalent to ours, but would be less useful for interpreting optical properties.

Finally, It we would like to mention that the isoelectronic substitution of one Au atom in $[Au_{13}Cl_2(dppe)_5]^{3+}$ by Hg^+ substantially disfavors configuration **I** (Figure 1). Indeed, the even lesser availability of the 5d(Hg) orbitals, as compared to 5d(Au), for for bonding with the Au_{12} cage, leads to an energetic preference by 27 kcal/mol for isomer **III**, i.e. Hg located at the M-Cl site, suggesting the possible extension to other doped species at different sites of the MAu_{12} core, besides the central position (Supporting information).

Concluding remarks

Here we predict the stabilization of 18-*ce* superatoms based on the central doping of the $M@Au_{12}Cl_2$ core, showing characteristic patterns for both UV/Vis and CD spectra. The optical properties are dominated by core–to–ligand charge transfer in contrast to the 8-*ce* cluster **1**, showing 1D → π*-ligand and 1P → π*-ligand character transitions. Such differences are also noted in the calculated CD spectra with a peak manifold between 950 and 650 nm, not observed for the parent Au_{13} cluster. The emission properties derived from the $T_1 \rightarrow S_1$ decay exhibit a red-shift from 809 nm calculated for **1** to 1045 nm for $[Os@Au_{12}(dppe)_5Cl_2]$, which involves an equatorial distortion of the $Au_{12}Cl_2$ core for the emissive excited state, rather than the axial distortion observed for **1**. The proposed neutral 18-*ce* $[M@Au_{12}(dppe)_5Cl_2]$ (M = Os, Ru, Fe) clusters exhibit weaker ligand–core interaction energy owing to a decrease in the ligand–core bonding interaction due to the extra $1D^{10}$ shell, denoting the smaller role of the protecting ligands to achieve stable species. The resulting sizable HOMO–LUMO gaps computed for these species indicate substantial stability. As already explored extensively for $MAu_{24}(SR)_{18}$ clusters, similar structural features are found for 8-*ce* and 18-*ce* species. This suggests further exploration of different doped species derived from the ligand-protected $Au_{12}Cl_2$ core that would allow to tuning molecular properties, and further designing novel building blocks for nanostructured materials under the superatom approach.

AUTHOR INFORMATION

Corresponding Authors

Jean-Yves Saillard*

jean-yves.saillard@univ-rennes1.fr

Alvaro Muñoz-Castro*

alvaro.munoz@uautonoma.cl

Authors

Jianyu Wei – orcid.org/0000-0001-8540-2233

P. L. Rodríguez-Kessler – orcid.org/0000-0003-2373-7729

Jean-Francọis Halet – orcid.org/0000-0002-2315-4200

Samia Kahlal - orcid.org/0000-0003-1121-0292
Jean-Yves Saillard orcid.org/0000-0003-4469-7922
Alvaro Muñoz-Castro orcid.org/0000-0001-5949-9449

Author Contributions

The manuscript was written through the contributions of all authors.

Acknowledgments

The authors are grateful to the Chilean-French ECOS-CONYCYT program (project C18E04 and ECOS180004) and to the French-Chilean International Associated Laboratory for “Multifunctional Molecules and Materials” (LIA-CNRS N°1027). The GENCI (Grand Equipment National de Calcul Intensif) is acknowledged for HCP support (project a0010807367). J.W. thanks the China Scholarship Council for a Ph.D. scholarship. A.M.-C. acknowledges support from Fondecyt 1180683. P.L.R.-K acknowledges to FONDECYT 3190329 grant.

References

(1) Levi-Kalisman, Y.; Jadzinsky, P. D.; Kalisman, N.; Tsunoyama, H.; Tsukuda, T.; Bushnell, D. A.; Kornberg, R. D. Synthesis and Characterization of Au102 (p-MBA) 44 Nanoparticles. *J. Am. Chem. Soc.* **2011**, *133* (9), 2976–2982.

(2) Tsukuda, T.; Tsunoyama, H.; Sakurai, H. Aerobic Oxidations Catalyzed by Colloidal Nanogold. *Chem. Asian J.* **2011**, *6* (3), 736–748. https://doi.org/10.1002/asia.201000611.

(3) Zhao, P.; Li, N.; Astruc, D. State of the Art in Gold Nanoparticle Synthesis. *Coord. Chem. Rev.* **2013**, *257* (3–4), 638–665. https://doi.org/10.1016/j.ccr.2012.09.002.

(4) Wuithschick, M.; Birnbaum, A.; Witte, S.; Sztucki, M.; Vainio, U.; Pinna, N.; Rademann, K.; Emmerling, F.; Kraehnert, R.; Polte, J. Turkevich in New Robes: Key Questions Answered for the Most Common Gold Nanoparticle Synthesis. *ACS Nano* **2015**, *9* (7), 7052–7071. https://doi.org/10.1021/acsnano.5b01579.

(5) Jin, R.; Zeng, C.; Zhou, M.; Chen, Y. Atomically Precise Colloidal Metal Nanoclusters and Nanoparticles: Fundamentals and Opportunities. *Chem. Rev.* **2016**, *116* (18), 10346–10413. https://doi.org/10.1021/acs.chemrev.5b00703.

(6) Weerawardene, K. L. D. M.; Aikens, C. M. Origin of Photoluminescence of $Ag_{25}(SR)_{18}^-$ Nanoparticles: Ligand and Doping Effect. *J. Phys. Chem. C* **2018**, *122* (4), 2440–2447. https://doi.org/10.1021/acs.jpcc.7b11706.

(7) Zhao, J.; Du, Q.; Zhou, S.; Kumar, V. Endohedrally Doped Cage Clusters. *Chem. Rev.* **2020**, *120* (17), 9021–9163. https://doi.org/10.1021/acs.chemrev.9b00651.

(8) Luo, Z.; Castleman, A. W.; Khanna, S. N. Reactivity of Metal Clusters. *Chem. Rev.* **2016**, *116* (23), 14456–14492. https://doi.org/10.1021/acs.chemrev.6b00230.

(9) Mingos, D. M. P. *Gold Clusters, Colloids and Nanoparticles I*; Mingos, D. M. P., Ed.; Structure and Bonding; Springer International Publishing: Cham, 2014; Vol. 161. https://doi.org/10.1007/978-3-319-07848-9.

(10) Mingos, D. M. P. *Gold Clusters, Colloids and Nanoparticles II*; Mingos, D. M. P., Ed.; Structure and Bonding; Springer International Publishing: Cham, 2014; Vol. 162. https://doi.org/10.1007/978-3-319-07845-8.

(11) Gao, Z.-H.; Dong, J.; Zhang, Q.-F.; Wang, L.-S. Halogen Effects on the Electronic and Optical Properties of Au 13 Nanoclusters. *Nanoscale Adv.* **2020**, *2* (10), 4902–4907. https://doi.org/10.1039/D0NA00662A.

(12) Kamei, Y.; Shichibu, Y.; Konishi, K. Generation of Small Gold Clusters with Unique Geometries through Cluster-to-Cluster Transformations: Octanuclear Clusters with Edge-Sharing Gold Tetrahedron Motifs. *Angew. Chem. Int. Ed.* **2011**, *50* (32), 7442–7445. https://doi.org/10.1002/anie.201102901.

(13) Zhu, Y.; Qian, H.; Jin, R. Catalysis Opportunities of Atomically Precise Gold Nanoclusters. *J. Mater. Chem.* **2011**, *21* (19), 6793. https://doi.org/10.1039/c1jm10082c.

(14) Kwak, K.; Kumar, S. S.; Lee, D. Selective Determination of Dopamine Using Quantum-Sized Gold Nanoparticles Protected with Charge Selective Ligands. *Nanoscale* **2012**, *4* (14), 4240–4246. https://doi.org/10.1039/c2nr30481c.

(15) Sakai, N.; Tatsuma, T. Photovoltaic Properties of Glutathione-Protected Gold Clusters Adsorbed on TiO(2) Electrodes. *Adv. Mater.* **2010**, *22* (29), 3185–3188. https://doi.org/10.1002/adma.200904317.

(16) Wu, Z.; Wang, M.; Yang, J.; Zheng, X.; Cai, W.; Meng, G.; Qian, H.; Wang, H.; Jin, R. Well-Defined Nanoclusters as Fluorescent Nanosensors: A Case Study on

Au(25) (SG)(18). *Small* **2012**, *8* (13), 2028–2035. https://doi.org/10.1002/smll.201102590.
(17) Murray, R. W. Nanoelectrochemistry: Metal Nanoparticles, Nanoelectrodes, and Nanopores. *Chem. Rev.* **2008**, *108* (7), 2688–2720. https://doi.org/10.1021/cr068077e.
(18) Galloway, J. M.; Bramble, J. P.; Rawlings, A. E.; Burnell, G.; Evans, S. D.; Staniland, S. S. Biotemplated Magnetic Nanoparticle Arrays. *Small* **2012**, *8* (2), 204–208. https://doi.org/10.1002/smll.201101627.
(19) Du, Y.; Sheng, H.; Astruc, D.; Zhu, M. Atomically Precise Noble Metal Nanoclusters as Efficient Catalysts: A Bridge between Structure and Properties. *Chem. Rev.* **2020**, *120* (2), 526–622. https://doi.org/10.1021/acs.chemrev.8b00726.
(20) Ebina, A.; Hossain, S.; Horihata, H.; Ozaki, S.; Kato, S.; Kawawaki, T.; Negishi, Y. One-, Two-, and Three-Dimensional Self-Assembly of Atomically Precise Metal Nanoclusters. *Nanomaterials* **2020**, *10* (6), 1105. https://doi.org/10.3390/nano10061105.
(21) Yao, Q.; Chen, T.; Yuan, X.; Xie, J. Toward Total Synthesis of Thiolate-Protected Metal Nanoclusters. *Acc. Chem. Res.* **2018**, *51* (6), 1338–1348. https://doi.org/10.1021/acs.accounts.8b00065.
(22) Sakthivel, N. A.; Dass, A. Aromatic Thiolate-Protected Series of Gold Nanomolecules and a Contrary Structural Trend in Size Evolution. *Acc. Chem. Res.* **2018**, *51* (8), 1774–1783. https://doi.org/10.1021/acs.accounts.8b00150.
(23) Aikens, C. M. Electronic and Geometric Structure, Optical Properties, and Excited State Behavior in Atomically Precise Thiolate-Stabilized Noble Metal Nanoclusters. *Acc. Chem. Res.* **2018**, *51* (12), 3065–3073. https://doi.org/10.1021/acs.accounts.8b00364.
(24) Ghosh, A.; Mohammed, O. F.; Bakr, O. M. Atomic-Level Doping of Metal Clusters. *Acc. Chem. Res.* **2018**, *51* (12), 3094–3103. https://doi.org/10.1021/acs.accounts.8b00412.
(25) Hossain, S.; Niihori, Y.; Nair, L. V.; Kumar, B.; Kurashige, W.; Negishi, Y. Alloy Clusters: Precise Synthesis and Mixing Effects. *Acc. Chem. Res.* **2018**, *51* (12), 3114–3124. https://doi.org/10.1021/acs.accounts.8b00453.
(26) Bhattarai, B.; Zaker, Y.; Atnagulov, A.; Yoon, B.; Landman, U.; Bigioni, T. P. Chemistry and Structure of Silver Molecular Nanoparticles. *Acc. Chem. Res.* **2018**, *51* (12), 3104–3113. https://doi.org/10.1021/acs.accounts.8b00445.
(27) Harb, M.; Rabilloud, F.; Simon, D. Structural, Electronic, Magnetic and Optical Properties of Icosahedral Silver–Nickel Nanoclusters. *Phys. Chem. Chem. Phys.* **2010**, *12* (16), 4246. https://doi.org/10.1039/b912971e.
(28) Yu, C.; Schira, R.; Brune, H.; von Issendorff, B.; Rabilloud, F.; Harbich, W. Optical Properties of Size Selected Neutral Ag Clusters: Electronic Shell Structures and the Surface Plasmon Resonance. *Nanoscale* **2018**, *10* (44), 20821–20827. https://doi.org/10.1039/C8NR04861D.
(29) Hossain, S.; Suzuki, D.; Iwasa, T.; Kaneko, R.; Suzuki, T.; Miyajima, S.; Iwamatsu, Y.; Pollitt, S.; Kawawaki, T.; Barrabés, N.; et al. Determining and Controlling Cu-Substitution Sites in Thiolate-Protected Gold-Based 25-Atom Alloy Nanoclusters. *J. Phys. Chem. C* **2020**, *124* (40), 22304–22313. https://doi.org/10.1021/acs.jpcc.0c06858.
(30) Xavier, P. L.; Chaudhari, K.; Baksi, A.; Pradeep, T. Protein-Protected Luminescent Noble Metal Quantum Clusters: An Emerging Trend in Atomic Cluster Nanoscience. *Nano Rev.* **2012**, *3* (1), 14767.

https://doi.org/10.3402/nano.v3i0.14767.
(31) Zhang, Q.-F.; Chen, X.; Wang, L.-S. Toward Solution Syntheses of the Tetrahedral Au20 Pyramid and Atomically Precise Gold Nanoclusters with Uncoordinated Sites. *Acc. Chem. Res.* **2018**, *51* (9), 2159–2168. https://doi.org/10.1021/acs.accounts.8b00257.
(32) Cook, A. W.; Hayton, T. W. Case Studies in Nanocluster Synthesis and Characterization: Challenges and Opportunities. *Acc. Chem. Res.* **2018**, *51* (10), 2456–2464. https://doi.org/10.1021/acs.accounts.8b00329.
(33) Lei, Z.; Wan, X.-K.; Yuan, S.-F.; Guan, Z.-J.; Wang, Q.-M. Alkynyl Approach toward the Protection of Metal Nanoclusters. *Acc. Chem. Res.* **2018**, *51* (10), 2465–2474. https://doi.org/10.1021/acs.accounts.8b00359.
(34) Sharma, S.; Chakrahari, K. K.; Saillard, J.-Y.; Liu, C. W. Structurally Precise Dichalcogenolate-Protected Copper and Silver Superatomic Nanoclusters and Their Alloys. *Acc. Chem. Res.* **2018**, *51* (10), 2475–2483. https://doi.org/10.1021/acs.accounts.8b00349.
(35) Higaki, T.; Li, Q.; Zhou, M.; Zhao, S.; Li, Y.; Li, S.; Jin, R. Toward the Tailoring Chemistry of Metal Nanoclusters for Enhancing Functionalities. *Acc. Chem. Res.* **2018**, *51* (11), 2764–2773. https://doi.org/10.1021/acs.accounts.8b00383.
(36) Tang, Q.; Hu, G.; Fung, V.; Jiang, D. Insights into Interfaces, Stability, Electronic Properties, and Catalytic Activities of Atomically Precise Metal Nanoclusters from First Principles. *Acc. Chem. Res.* **2018**, *51* (11), 2793–2802. https://doi.org/10.1021/acs.accounts.8b00380.
(37) Konishi, K.; Iwasaki, M.; Shichibu, Y. Phosphine-Ligated Gold Clusters with Core+exo Geometries: Unique Properties and Interactions at the Ligand–Cluster Interface. *Acc. Chem. Res.* **2018**, *51* (12), 3125–3133. https://doi.org/10.1021/acs.accounts.8b00477.
(38) Yan, J.; Teo, B. K.; Zheng, N. Surface Chemistry of Atomically Precise Coinage–Metal Nanoclusters: From Structural Control to Surface Reactivity and Catalysis. *Acc. Chem. Res.* **2018**, *51* (12), 3084–3093. https://doi.org/10.1021/acs.accounts.8b00371.
(39) Jin, R. Atomically Precise Metal Nanoclusters: Stable Sizes and Optical Properties. *Nanoscale* **2015**, *7* (5), 1549–1565. https://doi.org/10.1039/C4NR05794E.
(40) Zhu, M.; Aikens, C. M.; Hollander, F. J.; Schatz, G. C.; Jin, R. Correlating the Crystal Structure of A Thiol-Protected Au_{25} Cluster and Optical Properties. *J. Am. Chem. Soc.* **2008**, *130* (18), 5883–5885. https://doi.org/10.1021/ja801173r.
(41) Yuan, X.; Zhang, B.; Luo, Z.; Yao, Q.; Leong, D. T.; Yan, N.; Xie, J. Balancing the Rate of Cluster Growth and Etching for Gram-Scale Synthesis of Thiolate-Protected Au_{25} Nanoclusters with Atomic Precision. *Angew. Chem. Int. Ed.* **2014**, *53* (18), 4623–4627. https://doi.org/10.1002/anie.201311177.
(42) Kurashige, W.; Niihori, Y.; Sharma, S.; Negishi, Y. Precise Synthesis, Functionalization and Application of Thiolate-Protected Gold Clusters. *Coord. Chem. Rev.* **2016**, *320–321*, 238–250. https://doi.org/10.1016/j.ccr.2016.02.013.
(43) Chakraborty, I.; Pradeep, T. Atomically Precise Clusters of Noble Metals: Emerging Link between Atoms and Nanoparticles. *Chem. Rev.* **2017**, *117* (12), 8208–8271. https://doi.org/10.1021/acs.chemrev.6b00769.
(44) Kawawaki, T.; Imai, Y.; Suzuki, D.; Kato, S.; Kobayashi, I.; Suzuki, T.; Kaneko, R.; Hossain, S.; Negishi, Y. Atomically Precise Alloy Nanoclusters. *Chem. – A Eur. J.* **2020**, *26* (69), 16150–16193. https://doi.org/10.1002/chem.202001877.
(45) Negishi, Y.; Hashimoto, S.; Ebina, A.; Hamada, K.; Hossain, S.; Kawawaki, T.

Atomic-Level Separation of Thiolate-Protected Metal Clusters. *Nanoscale* **2020**, *12* (15), 8017–8039. https://doi.org/10.1039/D0NR00824A.

(46) Alkan, F.; Muñoz-Castro, A.; Aikens, C. M. C. M. Relativistic DFT Investigation of Electronic Structure Effects Arising from Doping the Au_{25} Nanocluster with Transition Metals. *Nanoscale* **2017**, *9* (41), 15825–15834. https://doi.org/10.1039/C7NR05214F.

(47) Ito, E.; Takano, S.; Nakamura, T.; Tsukuda, T. Controlled Dimerization and Bonding Scheme of Icosahedral M@Au_{12} (M=Pd, Pt) Superatoms. *Angew. Chem. Int. Ed.* **2021**, *60* (2), 645–649. https://doi.org/10.1002/anie.202010342.

(48) Qin, Z.; Sharma, S.; Wan, C.; Malola, S.; Xu, W.; Häkkinen, H.; Li, G. A Homoleptic Alkynyl-Ligated $[Au_{13}Ag_{16}L_{24}]^{3-}$ Cluster as a Catalytically Active Eight-Electron Superatom. *Angew. Chem. Int. Ed.* **2021**, *60* (2), 970–975. https://doi.org/10.1002/anie.202011780.

(49) Negishi, Y.; Kurashige, W.; Kobayashi, Y.; Yamazoe, S.; Kojima, N.; Seto, M.; Tsukuda, T. Formation of a Pd@Au12 Superatomic Core in Au 24Pd1(SC12H25)18 Probed by 197Au M??Ssbauer and Pd K-Edge EXAFS Spectroscopy. *J. Phys. Chem. Lett.* **2013**, *4* (21), 3579–3583. https://doi.org/10.1021/jz402030n.

(50) Kwak, K.; Tang, Q.; Kim, M.; Jiang, D. E.; Lee, D. Interconversion between Superatomic 6-Electron and 8-Electron Configurations of M@$Au_{24}(SR)_{18}$ Clusters (M = Pd, Pt). *J. Am. Chem. Soc.* **2015**, *137* (33), 10833–10840. https://doi.org/10.1021/jacs.5b06946.

(51) Juarez-Mosqueda, R.; Malola, S.; Häkkinen, H. Stability, Electronic Structure, and Optical Properties of Protected Gold-Doped Silver $Ag_{29-x}Au_x$ (x = 0–5) Nanoclusters. *Phys. Chem. Chem. Phys.* **2017**, *19* (21), 13868–13874. https://doi.org/10.1039/C7CP01440F.

(52) Alkan, F.; Pandeya, P.; Aikens, C. M. Understanding the Effect of Doping on Energetics and Electronic Structure for Au 25 , Ag 25 , and Au 38 Clusters. *J. Phys. Chem. C* **2019**, *123* (14), 9516–9527. https://doi.org/10.1021/acs.jpcc.9b00065.

(53) Tsukuda, T.; Häkkinen, H. *Protected Metal Clusters: From Fundamentals to Applications*; Elsevier, 2015.

(54) Jin, R.; Nobusada, K. Doping and Alloying in Atomically Precise Gold Nanoparticles. *Nano Res.* **2014**, *7* (3), 285–300. https://doi.org/10.1007/s12274-014-0403-5.

(55) Bhat, S.; Baksi, A.; Mudedla, S. K.; Natarajan, G.; Subramanian, V.; Pradeep, T. Au22Ir3(PET)18 : An Unusual Alloy Cluster through Intercluster Reaction. *J. Phys. Chem. Lett.* **2017**, 2787–2793. https://doi.org/10.1021/acs.jpclett.7b01052.

(56) Chai, J.; Lv, Y.; Yang, S.; Song, Y.; Zan, X.; Li, Q.; Yu, H.; Wu, M.; Zhu, M. X-Ray Crystal Structure and Optical Properties of $Au_{38-x}Cu_x$ $(2,4\text{-}(CH_3)_2C_6H_3S)_{24}$ (x = 0–6) Alloy Nanocluster. *J. Phys. Chem. C* **2017**, *121* (39), 21665–21669. https://doi.org/10.1021/acs.jpcc.7b05074.

(57) Omoda, T.; Takano, S.; Tsukuda, T. Toward Controlling the Electronic Structures of Chemically Modified Superatoms of Gold and Silver. *Small* **2020**, 2001439. https://doi.org/10.1002/smll.202001439.

(58) Walter, M.; Akola, J.; Lopez-Acevedo, O.; Jadzinsky, P. D.; Calero, G.; Ackerson, C. J.; Whetten, R. L.; Grönbeck, H.; Häkkinen, H.; Gronbeck, H.; et al. A Unified View of Ligand-Protected Gold Clusters as Superatom Complexes. *Proc. Natl. Acad. Sci.* **2008**, *105* (27), 9157–9162. https://doi.org/10.1073/pnas.0801001105.

(59) Castleman, A. W.; Khanna, S. N. Clusters, Superatoms, and Building Blocks of New Materials. *J. Phys. Chem. C* **2009**, *113* (7), 2664–2675. https://doi.org/10.1021/jp806850h.
(60) Jadzinsky, P. D.; Calero, G.; Ackerson, C. J.; Bushnell, D. A.; Kornberg, R. D. Structure of a Thiol Monolayer-Protected Gold Nanoparticle at 1.1 Å Resolution. *Science* **2007**, *318* (5849), 430–433. https://doi.org/10.1126/science.1148624.
(61) Claridge, S. A.; Castleman, A. W.; Khanna, S. N.; Murray, C. B.; Sen, A.; Weiss, P. S. Cluster-Assembled Materials. *ACS Nano* **2009**, *3* (2), 244–255. https://doi.org/10.1021/nn800820e.
(62) Bürgi, T. Properties of the Gold-Sulphur Interface: From Self-Assembled Monolayers to Clusters. *Nanoscale* **2015**, *7* (38), 15553–15567. https://doi.org/10.1039/C5NR03497C.
(63) Briant, C. E.; Theobald, B. R. C.; White, J. W.; Bell, L. K.; Mingos, D. M. P.; Welch, A. J. Synthesis and X-Ray Structural Characterization of the Centred Icosahedral Gold Cluster Compound $[Au_{13}(PMe_2Ph)_{10}Cl_2](PF_6)_3$; the Realization of a Theoretical Prediction. *J. Chem. Soc. Chem. Commun.* **1981**, No. 5, 201–202. https://doi.org/10.1039/c39810000201.
(64) Zhang, J.; Zhou, Y.; Zheng, K.; Abroshan, H.; Kauffman, D. R.; Sun, J.; Li, G. Diphosphine-Induced Chiral Propeller Arrangement of Gold Nanoclusters for Singlet Oxygen Photogeneration. *Nano Res.* **2017**, 1–12. https://doi.org/10.1007/s12274-017-1935-2.
(65) Shichibu, Y.; Konishi, K. HCl-Induced Nuclearity Convergence in Diphosphine-Protected Ultrasmall Gold Clusters: A Novel Synthetic Route to "Magic-Number" Au_{13} Clusters. *Small* **2010**, *6* (11), 1216–1220. https://doi.org/10.1002/smll.200902398.
(66) Ding, W.; Huang, C.; Guan, L.; Liu, X.; Luo, Z.; Li, W. Water-Soluble Au13 Clusters Protected by Binary Thiolates: Structural Accommodation and the Use for Chemosensing. *Chem. Phys. Lett.* **2017**, *676*, 18–24. https://doi.org/10.1016/j.cplett.2017.03.036.
(67) Sheong, F. K.; Zhang, J.-X.; Lin, Z. An $[Au_{13}]^{5+}$ Approach to the Study of Gold Nanoclusters. *Inorg. Chem.* **2016**, *55* (21), 11348–11353. https://doi.org/10.1021/acs.inorgchem.6b01881.
(68) Laupp, M.; Strähle, J. $[(Ph_3PAu)_6(DppeAu_2)(AuCl)_4Pd]$, an Icosahedral Au_{12} Cluster with a Central Pd Atom. *Angew. Chem. Int. Ed.* **1994**, *33* (2), 207–209. https://doi.org/10.1002/anie.199402071.
(69) Kang, X.; Chong, H.; Zhu, M. $Au_{25}(SR)_{18}$: The Captain of the Great Nanocluster Ship. *Nanoscale* **2018**, *10* (23), 10758–10834. https://doi.org/10.1039/C8NR02973C.
(70) Zhu, M.; Aikens, C. M.; Hendrich, M. P.; Gupta, R.; Qian, H.; Schatz, G. C.; Jin, R. Reversible Switching of Magnetism in Thiolate-Protected Au25 Superatoms. *J. Am. Chem. Soc.* **2009**, *131* (7), 2490–2492. https://doi.org/10.1021/ja809157f.
(71) Gam, F.; Paez-Hernandez, D.; Arratia-Perez, R.; Liu, C. W. W.; Kahlal, S.; Saillard, J.-Y. J.-Y.; Muñoz-Castro, A.; Gam, F.; Paez-Hernandez, D.; Arratia-Perez, R.; et al. Coinage Metal Superatomic Cores: Insights into Their Intrinsic Stability and Optical Properties from Relativistic DFT Calculations. *Chem. Eur. J.* **2017**, *23* (47), 11330–11337. https://doi.org/10.1002/chem.201701673.
(72) Saillard, J.-Y.; Halet, J.-F. Structure and Bonding Patterns in Large Molecular Ligated Metal Clusters. *Struct. Bond.* **2016**, *169*, 157–179. https://doi.org/10.1007/430_2015_210.
(73) Fehlner, T.; Halet, J.-F.; Saillard, J.-Y. Molecular Clusters. A Bridge to Solid

State Chemistry. *Cambridge Univ. Press. Cambridge, UK* **2007**.
(74) Häkkinen, H. Atomic and Electronic Structure of Gold Clusters: Understanding Flakes, Cages and Superatoms from Simple Concepts. *Chem. Soc. Rev.* **2008**, *37* (9), 1847–1859. https://doi.org/10.1039/b717686b.
(75) Mäkinen, V.; Koskinen, P.; Häkkinen, H. Modeling Thiolate-Protected Gold Clusters with Density-Functional Tight-Binding. *Eur. Phys. J. D* **2013**, *67* (2), 38. https://doi.org/10.1140/epjd/e2012-30486-4.
(76) Wen, F.; Englert, U.; Gutrath, B.; Simon, U. Crystal Structure, Electrochemical and Optical Properties of $[Au_9(PPh_3)_8](NO_3)_3$. *Eur. J. Inorg. Chem.* **2008**, *2008* (1), 106–111. https://doi.org/10.1002/ejic.200700534.
(77) Woehrle, G. H.; Warner, M. G.; Hutchison, J. E. Ligand Exchange Reactions Yield Subnanometer, Thiol-Stabilized Gold Particles with Defined Optical Transitions. *J. Phys. Chem. B* **2002**, *106* (39), 9979–9981. https://doi.org/10.1021/jp025943s.
(78) Schmid, G.; Pfeil, R.; Boese, R.; Bandermann, F.; Meyer, S.; Calis, G. H. M.; van der Velden, J. W. A. $Au_{55}[P(C_6H_5)3]_{12}Cl_6^{-}$ Ein Goldcluster Ungewöhnlicher Größe. *Chem. Ber.* **1981**, *114* (11), 3634–3642. https://doi.org/10.1002/cber.19811141116.
(79) Ashen-Garry, D.; Selke, M. Singlet Oxygen Generation by Cyclometalated Complexes and Applications. *Photochem. Photobiol.* **2014**, *90* (2), 257–274. https://doi.org/10.1111/php.12211.
(80) DeRosa, M. Photosensitized Singlet Oxygen and Its Applications. *Coord. Chem. Rev.* **2002**, *233–234*, 351–371. https://doi.org/10.1016/S0010-8545(02)00034-6.
(81) Mingos, D. M. P. Molecular-Orbital Calculations on Cluster Compounds of Gold. *J. Chem. Soc. Dalt. Trans.* **1976**, No. 13, 1163–1169. https://doi.org/10.1039/dt9760001163.
(82) Häkkinen, H. Electronic Structure: Shell Structure and the Superatom Concept. In *Protected Metal Clusters: From Fundamentals to Applications*; Hakkinen, H., Tsukuda, T., Eds.; Elsevier Science, 2015; pp 189–222. https://doi.org/10.1016/B978-0-08-100086-1.00008-7.
(83) Lopez-Acevedo, O.; Akola, J.; Whetten, R. L.; Grönbeck, H.; Häkkinen, H.; Gronbeck, H.; Ha kkinen, H. Structure and Bonding in the Ubiquitous Icosahedral Metallic Gold Cluster $Au_{144}(SR)_{60}$. *J. Phys. Chem. C* **2009**, *113* (13), 5035–5038. https://doi.org/10.1021/jp8115098.
(84) Kurashige, W.; Hayashi, R.; Wakamatsu, K.; Kataoka, Y.; Hossain, S.; Iwase, A.; Kudo, A.; Yamazoe, S.; Negishi, Y. Atomic-Level Understanding of the Effect of Heteroatom Doping of the Cocatalyst on Water-Splitting Activity in AuPd or AuPt Alloy Cluster-Loaded $BaLa_4Ti_4O_{15}$. *ACS Appl. Energy Mater.* **2019**, *2* (6), 4175–4187. https://doi.org/10.1021/acsaem.9b00426.
(85) Kumar, B.; Kawawaki, T.; Shimizu, N.; Imai, Y.; Suzuki, D.; Hossain, S.; Nair, L. V.; Negishi, Y. Gold Nanoclusters as Electrocatalysts: Size, Ligands, Heteroatom Doping, and Charge Dependences. *Nanoscale* **2020**, *12* (18), 9969–9979. https://doi.org/10.1039/D0NR00702A.
(86) Puls, A.; Jerabek, P.; Kurashige, W.; Förster, M.; Molon, M.; Bollermann, T.; Winter, M.; Gemel, C.; Negishi, Y.; Frenking, G.; et al. A Novel Concept for the Synthesis of Multiply Doped Gold Clusters $[(M@AunM'm)Lk]^{Q+}$. *Angew. Chem. Int. Ed.* **2014**, *53* (17), 4327–4331. https://doi.org/10.1002/anie.201310436.
(87) Negishi, Y.; Munakata, K.; Ohgake, W.; Nobusada, K. Effect of Copper Doping on Electronic Structure, Geometric Structure, and Stability of Thiolate-Protected Au_{25} Nanoclusters. *J. Phys. Chem. Lett.* **2012**, *3* (16), 2209–2214.

https://doi.org/10.1021/jz300892w.
(88) Negishi, Y.; Igarashi, K.; Munakata, K.; Ohgake, W.; Nobusada, K. Palladium Doping of Magic Gold Cluster $Au_{38}(SC_2H_4Ph)_{24}$: Formation of $Pd_2Au_{36}(SC_2H_4Ph)_{24}$ with Higher Stability than Au38(SC2H<sub>4</Su. *Chem. Commun.* **2012**, *48* (5), 660–662. https://doi.org/10.1039/C1CC15765E.
(89) Pyykkö, P.; Runeberg, N. Icosahedral WAu12: A Predicted Closed-Shell Species, Stabilized by Aurophilic Attraction and Relativity and in Accord with the 18-Electron Rule. *Angew. Chem. Int. Ed.* **2002**, *41* (12), 2174–2176. https://doi.org/10.1002/1521-3773(20020617)41:12<2174::AID-ANIE2174>3.0.CO;2-8.
(90) Li, X.; Kiran, B.; Li, J.; Zhai, H.-J.; Wang, L.-S. Experimental Observation and Confirmation of Icosahedral $W@Au_{12}$ and $Mo@Au_{12}$ Molecules. *Angew. Chem. Int. Ed.* **2002**, *41* (24), 4786–4789. https://doi.org/10.1002/anie.200290048.
(91) Hirai, H.; Takano, S.; Nakamura, T.; Tsukuda, T. Understanding Doping Effects on Electronic Structures of Gold Superatoms: A Case Study of Diphosphine-Protected $M@Au_{12}$ (M = Au, Pt, Ir). *Inorg. Chem.* **2020**, *59* (24), 17889–17895. https://doi.org/10.1021/acs.inorgchem.0c00879.
(92) Dyall, K. G.; Fægri, K. *Introduction to Relativistic Quantum Chemistry*; Oxford University Press, New York, 2007.
(93) Amsterdam Density Functional (ADF) Code, Vrije Universiteit: Amsterdam, The Netherlands. Http://Www.Scm.Com.
(94) van Lenthe, E.; Baerends, E.-J. J.; Snijders, J. G. Relativistic Total Energy Using Regular Approximations. *J. Chem. Phys.* **1994**, *101* (11), 9783. https://doi.org/10.1063/1.467943.
(95) Perdew, J. P.; Burke, K.; Wang, Y. Generalized Gradient Approximation for the Exchange-Correlation Hole of a Many-Electron System. *Phys. Rev. B* **1996**, *54* (23), 16533–16539. https://doi.org/10.1103/PhysRevB.54.16533.
(96) Perdew, J. P.; Burke, K.; Ernzerhof, M. Generalized Gradient Approximation Made Simple. *Phys. Rev. Lett.* **1997**, *78* (7), 1396–1396. https://doi.org/10.1103/PhysRevLett.78.1396.
(97) Akola, J.; Walter, M.; Whetten, R. L.; Häkkinen, H.; Grönbeck, H. On the Structure of Thiolate-Protected Au_{25}. *J. Am. Chem. Soc.* **2008**, *130* (12), 3756–3757. https://doi.org/10.1021/ja800594p.
(98) Jiang, D. The Expanding Universe of Thiolated Gold Nanoclusters and Beyond. *Nanoscale* **2013**, *5* (16), 7149–7160. https://doi.org/10.1039/c3nr34192e.
(99) Akola, J.; Kacprzak, K. A.; Lopez-Acevedo, O.; Walter, M.; Grönbeck, H.; Häkkinen, H. Thiolate-Protected Au_{25} Superatoms as Building Blocks: Dimers and Crystals. *J. Phys. Chem. C* **2010**, *114* (38), 15986–15994. https://doi.org/10.1021/jp1015438.
(100) Jiang, D.; Kühn, M.; Tang, Q.; Weigend, F. Superatomic Orbitals under Spin-Orbit Coupling. *J. Phys. Chem. Lett.* **2014**, *5* (19), 3286–3289. https://doi.org/10.1021/jz501745z.
(101) Grimme, S. Density Functional Theory with London Dispersion Corrections. *Wiley Interdiscip. Rev. Comput. Mol. Sci.* **2011**, *1* (2), 211–228. https://doi.org/10.1002/wcms.30.
(102) Versluis, L.; Ziegler, T. The Determination of Molecular Structures by Density Functional Theory. The Evaluation of Analytical Energy Gradients by Numerical Integration. *J. Chem. Phys.* **1988**, *88* (1), 322–328. https://doi.org/10.1063/1.454603.
(103) Lopez-Acevedo, O.; Tsunoyama, H.; Tsukuda, T.; Häkkinen, H.; Aikens, C. M.;

Häkkinen, H.; Aikens, C. M. Chirality and Electronic Structure of the Thiolate-Protected Au_{38} Nanocluster. *J. Am. Chem. Soc.* **2010**, *132* (23), 8210–8218. https://doi.org/10.1021/ja102934q.

(104) Ai, P.; Mauro, M.; Danopoulos, A. A. A. A.; Muñoz-Castro, A.; Braunstein, P. Dual Emission of a Cyclic Hexanuclear Gold(I) Complex. Interplay between Au_3 and Au_2 Ligand-Supported Luminophores. *J. Phys. Chem. C* **2019**, *123* (1), 915–921. https://doi.org/10.1021/acs.jpcc.8b10190.

(105) Mingos, D. M. P.; Zhenyang, L. Site Preference Effects in Heterometallic Clusters. *Comments Inorg. Chem.* **1989**, *9* (2), 95–122. https://doi.org/10.1080/02603598908035805.

(106) Morokuma, K. Molecular Orbital Studies of Hydrogen Bonds. III. C=O···H–O Hydrogen Bond in $H_2CO\cdots H_2O$ and $H_2CO\cdots 2H_2O$. *J. Chem. Phys.* **1971**, *55* (3), 1236–1244. https://doi.org/10.1063/1.1676210.

(107) Ziegler, T.; Rauk, A. Calculation of Bonding Energies by Hartree-Fock Slater Method. 1. Transition-State Method. *Theor. Chim. Acta* **1977**, *46* (1), 1–10.

(108) Hopffgarten, M. von; Frenking, G.; von Hopffgarten, M.; Frenking, G. Energy Decomposition Analysis. *Wiley Interdiscip. Rev. Comput. Mol. Sci.* **2012**, *2* (1), 43–62. https://doi.org/10.1002/wcms.71.

(109) MacLeod Carey, D.; Muñoz-Castro, A. Evaluation of N-Heterocyclic Carbene Counterparts of Classical Gold Clusters; Bonding Properties of Octahedral CAu_6, Icosahedral $Au_{13}Cl_2$, and Bi-Icosahedral $Au_{25}Cl_2$ Cores from Relativistic DFT Calcula. *J. Phys. Chem. C* **2019**, *123* (19), 12466–12473. https://doi.org/10.1021/acs.jpcc.9b01254.

(110) Muñoz-Castro, A. Potential of N-Heterocyclic Carbene Derivatives from $Au_{13}(Dppe)_5Cl_2$ Gold Superatoms. Evaluation of Electronic, Optical and Chiroptical Properties from Relativistic DFT. *Inorg. Chem. Front.* **2019**, *6* (9), 2349–2358. https://doi.org/10.1039/C9QI00513G.

(111) Du, L.; Furube, A.; Hara, K.; Katoh, R.; Tachiya, M. Ultrafast Plasmon Induced Electron Injection Mechanism in Gold–TiO_2 Nanoparticle System. *J. Photochem. Photobiol. C Photochem. Rev.* **2013**, *15*, 21–30. https://doi.org/10.1016/j.jphotochemrev.2012.11.001.

(112) Mingos, D. M. P.; Lewis, J.; Green, M. L. H. Some Theoretical and Structural Aspects of Gold Cluster Chemistry. *Philos. Trans. R. Soc. London. Ser. A, Math. Phys. Sci.* **1982**, *308* (1501), 75–83. https://doi.org/10.1098/rsta.1982.0148.

(113) Hall, K. P.; Mingos, D. M. P. Homo- and Heteronuclear Cluster Compounds of Gold. In *Progress in Inorganic Chemistry*; 1984; pp 237–325. https://doi.org/10.1002/9780470166338.ch3.

TOC